Inorganic Chemistry

ARTICLE

pubs.acs.org/IC

Lanthanoid-Containing Open Wells−Dawson Silicotungstates: Synthesis, Crystal Structures, and Properties

Lubin Ni,[†] Firasat Hussain,[†,‡] Bernhard Spingler,[†] Stephen Weyeneth,[§] and Greta R. Patzke*[,†]

[†]Institute of Inorganic Chemistry, University of Zurich, Winterthurerstrasse 190, CH-8057 Zurich, Switzerland

[‡]Department of Chemistry, University of Delhi, 110 007 Delhi, India

[§]Physik-Institut der Universität Zürich, Winterthurerstrasse 190, CH-8057 Zürich, Switzerland

Supporting Information

ABSTRACT: Five novel lanthanoid-containing silicotungstates with polymeric crystal structures $[Ln_2(H_2O)_7Si_2W_{18}O_{66}]_n^{10n-}$ [Ln = Gd^{III} (**Gd-1** and **Gd-2**), Tb^{III}, Ho^{III}] and $[Dy_2(H_2O)_{6.5}(C_2H_4O_2)_{0.5}Si_2W_{18}O_{66}]_n^{10n-}$ were obtained from the one-step reaction of $Na_{10}[SiW_9O_{34}]\cdot nH_2O$ with $Ln(NO_3)_3\cdot nH_2O$ in a sodium acetate buffer. The compounds were characterized by single-crystal X-ray diffraction and a wide range of analytical methods, including FT-IR, UV/vis, and photoluminescence spectroscopy as well as electrochemistry and thermogravimetric analysis. This new polyoxotungstate series is the first example of lanthanoids embedded in the open Wells−Dawson silicotungstate anion $[\alpha\text{-}Si_2W_{18}O_{66}]^{16-}$. The lanthanoid-containing Wells−Dawson-type polyoxoanions $[Ln_2(H_2O)_7Si_2W_{18}O_{66}]^{10-}$ [Ln = Gd^{III} (**Gd-1** and **Gd-2**), Tb^{III}, Ho^{III}] and $[Dy_2(H_2O)_{6.5}(C_2H_4O_2)_{0.5}Si_2W_{18}O_{66}]^{10-}$ are linked by Ln^{3+} cations to form 3D architectures for **Gd-1** or 2D frameworks for the isostructural compounds **Tb-2**, **Dy-2**, **Ho-2**, and **Gd-2**. The structure-directing influence of the lanthanoid cation on the local structure of the dimeric building blocks and on the crystal packing motifs is investigated in detail. The photoluminescence properties of **Tb-2** and **Dy-2** were investigated at room temperature, and **Ho-2** exhibits an interesting photochromic behavior. The magnetic susceptibility of **Gd-1** and **Gd-2** was studied in the temperature range between 2 and 300 K for its effective magnetic moment.

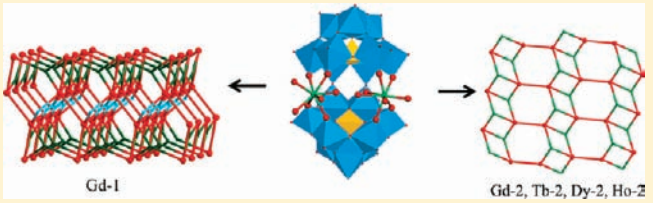

INTRODUCTION

Polyoxometalates (POMs) are transition-metal oxide nanoclusters (usually of V, W, and Mo in their high oxidation states) that provide an exceptional variety of structural motifs from solution-based approaches in aqueous media. The manifold potential POM applications arising from their infinite number of molecular architectures are now widely investigated, e.g., in the fields of medicine, catalysis, water splitting, imaging techniques, multifunctional materials, or bio- and nanotechnology.[1−13] Lanthanoid-containing POMs are of special interest with respect to key magnetic properties, luminescence, and Lewis acid catalysis, and Gd POMs, in particular, are used for the development of magnetic resonance imaging agents.[14] We have thus explored the reactivity of lanthanoid cations with different types of lacunary POMs,[15] and this synthetic strategy has proven rather fruitful: First, lacunary POMs and large oxophilic lanthanoid cations can be readily combined into high nuclear polyoxoanion complexes with unprecedented structures, sizes, and new properties. Second, lanthanoid cations are particularly efficient linkers because of their high coordination numbers and flexible coordination geometries. Therefore, this method is generally favorable for constructing polymeric or unusually large POM assemblies.

This is illustrated by Pope et al.'s high-nuclear cerium-containing polyoxotungstoarsenate(III) $[Ce_{16}As_{12}(H_2O)_{36}W_{148}O_{524}]^{76-}$, which has long been the largest polyoxotungstate ever observed,[16] followed by Kortz et al.'s synthesis of $[Ce_{20}Ge_{10}W_{100}O_{376}(OH)_4(H_2O)_{30}]^{56-}$.[17] Recently, our group has amplified the spectrum of lanthanoid linkers to middle and late members of the series,[18] as represented by the $[Cs\subset Ln_6As_6W_{63}O_{218}(H_2O)_{14}(OH)_4]^{25-}$ type (Ln = Eu, Gd, Tb, Dy, Ho, Er) and the $[Gd_8As_{12}W_{124}O_{432}(H_2O)_{22}]^{60-}$ polyanion.[15a,b] Our efforts finally resulted in the $[Ln_{16}As_{16}W_{164}O_{576}(OH)_8(H_2O)_{42}]^{80-}$ (Ln = Eu, Gd, Tb, Dy, Ho) family with the largest number of tungsten centers to date.[15c] Related studies are performed by the groups of Müller, Francesconi, Yamase, Krebs, Kortz, Gouzerh, Sécheresse, Hill, and others.[19] As shown in our present work, however, the inexhaustible structural variety of lanthanoid-containing POM structures, ranging from discrete building blocks to polymeric arrangements, can only be tapped by a comparable flexibility of synthetic approaches.

Although the reactivity of the monovacant silicotungstate $[SiW_{11}O_{39}]^{8-}$ with trivalent lanthanoids leading to the formation of 1D inorganic chains or 2D layers has been well investigated by Peacock,[20] Pope,[21] Mialane,[22] Kortz,[23] and Niu[24] and their respective co-workers, no studies on the conversion of the trilacunary Keggin polyoxoanion $[SiW_9O_{34}]^{10-}$ into Wells−Dawson $[Si_2W_{18}O_{66}]^{16-}$ ions in the presence of lanthanoid cations have been reported. Furthermore, only a few 3D inorganic

Received: January 27, 2011
Published: May 10, 2011

architectures of lanthanoid-containing POMs are known up to now. Two Keggin-type monolacunary polyoxotungstoborates $[Ln(H_2O)(BW_{11}O_{39}H)]^{10-}$ (Ln = Ce, Nd) have been recently discovered by An and co-workers.[25] In the following, we report on the reactivity of the $[A\text{-}\alpha\text{-}SiW_9O_{34}]^{10-}$ precursor in the presence of different lanthanoid cations. We successfully obtained five polymeric Ln-based POMs (Ln = Gd, Tb, Dy, Ho) from the incorporation of lanthanoid cations into the open Wells–Dawson anion $[\alpha\text{-}Si_2W_{18}O_{66}]^{16-}$, which was first characterized by Hervé et al.[26,27] The potassium salt of $[Si_2W_{18}O_{66}]^{16-}$, furthermore, serves as a precursor for the formation of the silicotungstate polyanions $\alpha\text{-}[\{[K(H_2O)_2(\mu\text{-}H_2O)\text{-}[Li(H_2O)_2]\}_2Si_4W_{36}O_{126}(H_2O)_2]^{16-}$ and $\alpha\text{-}[\{[K(H_2O)][K(H_2O)_4]\}_2Si_8W_{36}O_{136}]^{22-}$ through a stepwise self-assembly process.[28] The open Wells–Dawson anion can intercalate two transition-metal cations (Mn, Co, Ni, Cu) in addition to the K^+ ion present in the pocket, resulting in different coordination modes[28] (cf. Table S1 in the Supporting Information for a survey of related compounds). Later, Hervé and co-workers accessed polyanions with dinuclear $\{KV_2O(H_2O)_2\}^{5+}$ and tetranuclear $\{Fe_4(OH)_6\}^{6+}$ moieties included in the pocket between the two $[\alpha\text{-}Si_2W_{18}O_{66}]^{16-}$ subunits through reaction of the open Wells–Dawson anion with V^V and Fe^{III} cations.[29] In 2004, Kortz et al. synthesized a pentacopper-substituted polyanion, with the copper oxo cluster $\{Cu_5(OH)_4(H_2O)\}^{6+}$ perfectly fitting into the cavity of the open Wells–Dawson anion.[30] The same group also discovered monosubstituted transition-metal derivatives of $\gamma\text{-}[Si_2W_{20}O_{70}]^{12-}$.[31]

The title compounds are all constituted of the novel dimeric polyoxoanion $[Ln_2(H_2O)_7Si_2W_{18}O_{66}]^{10-}$ [Ln = Gd^{III} (**Gd-1** and **Gd-2**), Tb^{III}, Ho^{III}] and $[Dy_2(H_2O)_{6.5}(C_2H_4O_2)_{0.5}Si_2W_{18}O_{66}]^{10-}$, respectively, which consist of two lanthanoid cations within the open Wells–Dawson units. These polyoxoanion moieties are further linked by Ln^{3+} cations into 3D or 2D architectures. The influence of the cationic radii on the local structure of the POM as well as on the 3D packing motifs of the compounds is discussed. The photoluminescent properties of the terbium- and dysprosium-containing polyanions were investigated at room temperature. All compounds were electrochemically characterized in a sodium acetate buffer (pH 4.4) solution as the supporting electrolyte.

EXPERIMENTAL SECTION

Materials and Analytical Methods. The $Na_{10}[A\text{-}\alpha\text{-}SiW_9O_{34}]\cdot 23H_2O$ precursor was prepared according to literature protocols[32] and characterized with IR spectroscopy. All other chemicals were commercially purchased and used without further purification. Elemental analyses of all polyanions were performed by Mikroanalytisches Labor Pascher, Remagen, Germany. Fourier transform infrared (FT-IR) spectra were recorded on a Perkin-Elmer BXII spectrometer with KBr pellets. Thermogravimetric analysis (TGA) measurements were performed on a Netzsch STA 449 C between 30 and 800 °C with a heating rate of 5 K min^{-1} in a nitrogen atmosphere. UV/vis spectra were recorded on a Perkin-Elmer Lambda 650S spectrometer. Powder X-ray diffraction (PXRD) data were recorded on a Philips X'Pert PRO diffractometer, operated at 40 kV and 30 mA (Cu $K\alpha_1$ radiation). Photoluminescence measurements were performed on a Perkin-Elmer LS 50B spectrometer. Magnetic measurements were performed with a SQUID magnetometer (Quantum Design, MPMS-7) in the temperature range 2–300 K with an applied magnetic field of 2 kOe. Here a small temperature-independent contribution to the paramagnetic susceptibility, stemming from the electronic susceptibility of the sample and from the sample holder configuration, was subtracted from the data prior to further analysis (-1.54×10^{-3} emu Oe^{-1} mol^{-1} for **Gd-1** and -5.38×10^{-4} emu Oe^{-1} mol^{-1} for **Gd-2**). Cyclic voltammetry (CV) measurements were performed using a Metrohm Computrace model 757 VA voltammetric analyzer. The system was operated using 757 VA Computrace software (Metrohm). The three-electrode cell system consisted of a 2 mm glassy carbon working electrode (modified or unmodified), a saturated Ag/AgCl reference electrode, and a platinum wire counter electrode.

Synthesis of $Na_2CsCaGd_2[Gd_2(H_2O)_7Si_2W_{18}O_{66}]Cl\cdot 27H_2O$ (Gd-1). A total of 0.369 g (0.150 mmol) of $Na_{10}[SiW_9O_{34}]\cdot 23H_2O$ was dissolved in 25 mL of a sodium acetate buffer (pH 4.4) with stirring. A total of 0.203 g (0.450 mmol) of $Gd(NO_3)\cdot 6H_2O$ was slowly added to the reaction mixture. The solution was stirred continuously at 80 °C for 90 min, followed by cooling to room temperature and filtering. The addition of a 1.0 M CsCl solution (0.5 mL) to the colorless filtrate and slow evaporation at room temperature led to the formation of colorless needlelike crystals after about 1 week. Yield: 21.0% (based on $Na_{10}[A\text{-}\alpha\text{-}SiW_9O_{34}]\cdot 23H_2O$). FT-IR ($cm^{-1}$): 1001 (s), 938 (s), 871 (vs), 833 (s), 808 (s), 723 (s), 555 (w), 529 (w). Elem anal. Calcd (found): W, 55.92 (55.20); Gd, 10.63 (11.00); Cs, 2.25 (3.10); Na, 0.78 (0.63); H, 1.16 (1.13). The number of water molecules has been confirmed by TGA (cf. Figure S5 in the Supporting Information).

Synthesis of $Na_2Cs_3H_2Tb[Tb_2(H_2O)_7Si_2W_{18}O_{66}]\cdot 17H_2O$ (Tb-2). The above synthetic procedure was modified by using 0.196 g (0.450 mmol) of $Tb(NO_3)_3\cdot 5H_2O$ instead of $Gd(NO_3)_3\cdot 6H_2O$. Colorless block-shaped crystals were obtained after about 1 week. Yield: 13.8% (based on $Na_{10}[A\text{-}\alpha\text{-}SiW_9O_{34}]\cdot 23H_2O$). FT-IR ($cm^{-1}$): 1002 (s), 937 (s), 876 (vs), 818 (s), 718 (s), 547 (w), 524 (w). Elem anal. Calcd (found): W, 57.28 (54.20); Tb, 8.25 (8.77); Cs, 6.90 (6.74); Na, 0.80 (1.00); H, 0.87 (0.99). The number of water molecules has been confirmed by TGA (cf. Figure S5 in the Supporting Information).

Synthesis of $Na_4Cs_3DyH[Dy_2(H_2O)_{6.5}(C_2H_4O_2)_{0.5}Si_2W_{18}O_{66}]Cl\cdot 17H_2O$ (Dy-2). The above synthetic procedure was applied using 0.197 g (0.450 mmol) of $Dy(NO_3)_3\cdot 5H_2O$ instead of $Gd(NO_3)_3\cdot 6H_2O$. Colorless blocklike crystals were obtained after about 1 week. Yield: 15.2% (based on $Na_{10}[A\text{-}\alpha\text{-}SiW_9O_{34}]\cdot 23H_2O$). FT-IR ($cm^{-1}$): 1002 (s), 940 (s), 882 (vs), 817 (s), 716 (s), 551 (w), 528 (w). Elem anal. Calcd (found): W, 56.19 (53.30); Dy, 8.27 (8.11); Cs, 6.77 (7.05); Na, 1.56 (1.61); H, 0.85 (0.99); C, 0.20 (0.16). The number of water molecules has been confirmed by TGA (cf. Figure S5 in the Supporting Information).

Synthesis of $Na_4Cs_3Ho[Ho_2(H_2O)_7Si_2W_{18}O_{66}]\cdot 18H_2O$ (Ho-2). The above synthetic procedure was performed with 0.200 g (0.450 mmol) of $Ho(NO_3)_3\cdot 5H_2O$ instead of $Gd(NO_3)_3\cdot 6H_2O$. Light-pink block-shaped crystals were obtained after about 1 week. Yield: 12.4% (based on $Na_{10}[A\text{-}\alpha\text{-}SiW_9O_{34}]\cdot 23H_2O$). FT-IR ($cm^{-1}$): 1003 (s), 939 (s), 868 (vs), 833 (s), 809 (s), 714 (s), 555 (w), 529 (w). Elem. anal. Calcd (found): W, 56.50 (54.00); Ho, 8.44 (8.68); Cs, 6.81 (6.68); Na, 1.57 (1.58); H, 0.86 (0.98). The number of water molecules has been confirmed by TGA (cf. Figure S5 in the Supporting Information).

Synthesis of $Na_{2.5}Cs_{3.5}GdH_2[Gd_2(H_2O)_7Si_2W_{18}O_{66}](C_2H_3O_2)\cdot 16H_2O$ (Gd-2). The synthetic procedure was conducted as described above for **Gd-1** with one alteration: instead of 0.5 mL of a 1.0 M CsCl solution, 1.2 mL was added to the colorless filtrate dropwise. Colorless blocklike crystals were obtained after about 1 week. Yield: 15.6% (based on $Na_{10}[A\text{-}\alpha\text{-}SiW_9O_{34}]\cdot 23H_2O$). FT-IR ($cm^{-1}$): 1002 (s), 934 (s), 886 (vs), 814 (s), 720 (s), 551(w), 529(w). Elem anal. Calcd (found): W, 56.17 (54.50); Gd, 8.00 (7.68); Cs, 7.30 (7.41); Na, 0.97 (1.09); C, 0.41 (0.40); H, 0.86 (0.70). The number of water molecules has been confirmed by TGA (cf. Figure S5 in the Supporting Information).

X-ray Crystallography. Data collection of compounds **Gd-1**, **Gd-2**, **Tb-2**, **Dy-2**, and **Ho-2** was performed on an Oxford Xcalibur Ruby CCD single-crystal diffractometer (Mo $K\alpha$ radiation, $\lambda = 0.710\,73$ Å) at 183(2) K. Lorentz and polarization corrections were applied, and an

dx.doi.org/10.1021/ic2001943 |Inorg. Chem. 2011, 50, 4944–4955

Table 1. Crystallographic Data for Compounds Gd-1, Gd-2, Tb-2, Dy-2, and Ho-2

	Gd-1	Gd-2	Tb-2	Dy-2	Ho-2
empirical formula	$CsCaH_{68}Na_2Gd_4O_{100}Si_2W_{18}Cl$	$C_2Cs_{3.5}H_{51}Gd_3Na_{2.5}O_{91}Si_2W_{18}$	$Cs_3H_{50}Na_2Tb_3O_{90}Si_2W_{18}$	$CCs_3H_{50}Dy_3Na_4O_{90.5}Si_2W_{18}C1$	$Cs_3H_{50}Ho_3Na_4O_{91}Si_2W_{18}$
fw (g mol^{-1})	5917.18	5890.84	5777.10	5888.93	5857.12
T (K)	183(2)	183(2)	183(2)	183(2)	183(2)
λ (Å)	0.710 73	0.710 73	0.710 73	0.710 73	0.710 73
cryst syst, space group	monoclinic, $C2/c$	triclinic, $P\bar{1}$	triclinic, $P\bar{1}$	triclinic, $P\bar{1}$	triclinic, $P\bar{1}$
a (Å)	26.1719(4)	12.8242(1)	12.9462(2)	12.8335(3)	12.9422(12)
b (Å)	20.7408(4)	15.7895(2)	15.7702(2)	15.7343(3)	15.6464(8)
c (Å)	39.3620(8)	23.2486(3)	23.1831(3)	23.1443(4)	23.0735(12)
α (deg)	90.00	99.591(1)	99.135(1)	99.304(2)	99.062(4)
β (deg)	94.021(2)	97.904(1)	98.002(2)	98.206(2)	98.117(6)
γ (deg)	90.00	91.547(1)	93.398(1)	92.871(2)	93.777(6)
V (Å^3)	21314.1(7)	4591.65(9)	4611.6(1)	4551.9(1)	4549.2(5)
Z	8	2	2	2	2
abs coeff (mm^{-1})	22.476	26.064	25.939	26.248	26.318
d_{calcd} (Mg m^{-3})	3.719	4.307	4.263	4.293	4.226
F(000)	20756	5141	5116	5085	4992
cryst size (mm)	0.38 × 0.06 × 0.04	0.15 × 0.08 × 0.05	0.23 × 0.22 × 0.13	0.23 × 0.18 × 0.06	0.11 × 0.09 × 0.08
GOF on F^2	0.885	0.996	1.065	0.921	0.916
R1 [$I > 2\sigma(I)$][a]	0.0490	0.0384	0.0414	0.0401	0.0515
wR2 [$I > 2\sigma(I)$][a]	0.0914	0.0906	0.0986	0.0837	0.1075

[a] $R1 = \Sigma(F_o - F_c)/\Sigma F_o$ and $wR2 = \{\Sigma w(F_o^2 - F_c^2)^2/\Sigma w(F_o^2)^2\}^{1/2}$.

absorption correction was performed using the program *CrysAlis*.[33] Direct methods were used to locate the heavy-metal atoms (*SHELXS-97*). The remaining atoms were located from successive Fourier maps (*SHELXL-97*).[34] Further details on the crystal structure data can be obtained from ICSD/FIZ Karlsruhe via www.fiz-karlsruhe.de/icsd.html [fax (+49) 7247-808-666; e-mail crysdata@fiz-karlsruhe.de], on quoting the depository numbers CSD 422265−422268 for **Gd-1**, **Tb-2**, **Dy-2**, and **Ho-2**, respectively, and 422404 for **Gd-2**. All heavy atoms were refined anisotropically except for some disordered alkali-metal counterions and free water molecules. The incorporation of one calcium cation into **Gd-1** was deduced from the crystallographic environment of this specific position. Because the calcium content determined from experimental analyses is considerably lower, the selected single crystal probably deviates in this minor detail from the bulk material that is otherwise in good agreement with elemental analysis results for the main constituting elements. As a consequence, the experimental PXRD of **Gd-1** (Figure S10 in the Supporting Information) does not display a very convincing match with the theoretical pattern calculated from the X-ray crystallographic data. It is also noteworthy that the PXRD of **Gd-1** displays the lowest crystallinity among the series (cf. Figures S10−S14 in the Supporting Information), which is in line with the hypothesis that Ca^{2+} selectively promotes single crystal growth. **Gd-2** contains an obvious site-occupancy disorder of Cs3, which has been refined on two positions with site occupancies of 0.6 and 0.4. The Tb1 atom in **Tb-2** exhibits disorder over two positions that were refined with site occupancies of 0.8 and 0.2, respectively, and the Na1 split positions in **Tb-2** were described with site occupancies of 0.7 and 0.3. The half-occupied Cs4 atom in **Tb-2** exhibits disorder over two positions that were refined with site occupancies of 0.3 and 0.2. **Dy-2** also exhibits disorder, namely, of Na2, on two positions with relative occupancies of 0.6 and 0.4, and the Cl1 atom is disordered into two positions with an occupancy of 0.5. In all of the structures, there is a discrepancy between the formulas determined by elemental analysis and those deduced from the crystallographic atom list. This is due to considerable disorder among the cations and the water molecules, which is a common phenomenon encountered in POM chemistry. Hydrogen atoms were not included in the refinements. The crystallographic data of all polyanions are summarized in Table 1.

RESULTS AND DISCUSSION

Synthetic Strategy. We reacted the silicotungstate precursor $Na_{10}[A\text{-}\alpha\text{-}SiW_9O_{34}]\cdot 23H_2O$ ({α-SiW_9}) with lanthanide cations (Ln = Gd^{III}, Ho^{III}, Tb^{III}, Dy^{III}) under optimized reaction conditions. Five polymeric polyanions with two framework-based structures were successfully isolated in a 1.0 M sodium acetate buffer (pH 4.4) at 80 °C by combining {α-SiW_9} and Ln^{3+} cations in a molar ratio of 1:3 for 90 min. The solution was cooled to room temperature, subsequently filtered off, and set for crystallization.

Slow evaporation at room temperature yielded crystals suitable for single-crystal X-ray diffraction, followed by FT-IR and UV/vis spectroscopy, CV and photoluminescence measurements, TGA, and elemental analysis. The polymeric polyanions were isolated as mixed sodium/cesium salts: $Na_2CsCaGd_2[Gd_2(H_2O)_7Si_2W_{18}O_{66}]Cl\cdot 27H_2O$ (**Gd-1**), $Na_{2.5}Cs_{3.5}GdH_2[Gd_2(H_2O)_7Si_2W_{18}O_{66}](C_2H_3O_2)\cdot 16H_2O$ (**Gd-2**), $Na_2Cs_3H_2Tb[Tb_2(H_2O)_7Si_2W_{18}O_{66}]\cdot 17H_2O$ (**Tb-2**), $Na_4Cs_3DyH[Dy_2(H_2O)_{6.5}(C_2H_4O_2)_{0.5}Si_2W_{18}O_{66}]Cl\cdot 17H_2O$ (**Dy-2**), and $Na_4Cs_3Ho[Ho_2(H_2O)_7Si_2W_{18}O_{66}]\cdot 18H_2O$ (**Ho-2**).

Both **Gd-1** with a 3D inorganic framework and **Gd-2**−**Ho-2** with 2D layer networks are constituted of dimeric building blocks consisting of two $[A\text{-}\alpha\text{-}SiW_9O_{34}]^{10-}$ fragments, which are connected through W−O−W bonds via two axial oxygen atoms of each individual anion. The W−O−W bonds are bent toward the interior of the polyanion, thereby forming the pocket of the open Wells−Dawson ion $[\alpha\text{-}Si_2W_{18}O_{66}]^{16-}$. The multilacunary polyanions of compounds **Gd-1** to **Ho-2** have incorporated two lanthanoid cations within their structural cavities to form the

dx.doi.org/10.1021/ic2001943 |*Inorg. Chem.* 2011, 50, 4944–4955

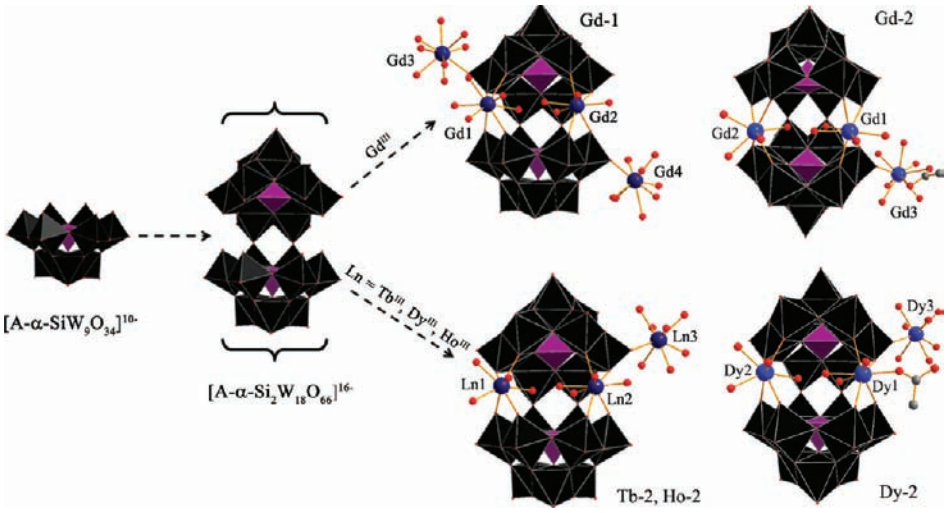

Figure 1. Transformation of the $[A\text{-}\alpha\text{-}SiW_9O_{34}]^{10-}$ precursor into dimeric $[Ln_2(H_2O)_7Si_2W_{18}O_{66}]^{10-}$ [Ln = Gd^{III} (**Gd-1** and **Gd-2**), Tb^{III}, Ho^{III}] and $[Dy_2(H_2O)_{6.5}(C_2H_4O_2)_{0.5}Si_2W_{18}O_{66}]^{10-}$ polyanions in a HOAc/NaOAc buffer (W, black polyhedra; Si, purple polyhedra; Ln, blue; O, red; C, gray).

dimeric building blocks $[Ln_2(H_2O)_7Si_2W_{18}O_{66}]^{10-}$ (Ln = Gd, Ho, Tb) and $[Dy_2(H_2O)_{6.5}(C_2H_4O_2)_{0.5}Si_2W_{18}O_{66}]^{10-}$. These moieties are, furthermore, linked to external lanthanoid atoms via terminal oxygen atoms of the neighboring polyanion (W=O), thereby forming two different framework types (**Gd-1** and **Gd-2**—**Ho-2**, respectively; cf. Figure 1).

It is noteworthy that previous syntheses of the parent anion were based on potassium salts, which suggests an essential role of K^+ in maintaining the open Wells—Dawson structure with its special coordination sites for different cations.[26,27,29] In the case of the newly formed $[Ln_2(H_2O)_7Si_2W_{18}O_{66}]^{10-}$ [Ln = Gd^{III} (**Gd-1** and **Gd-2**), Tb^{III}, Ho^{III}] and $[Dy_2(H_2O)_{6.5}(C_2H_4O_2)_{0.5}Si_2W_{18}O_{66}]^{10-}$ polyanions, the lanthanoids occupy the peripheral K^+ position in the $[\alpha\text{-}Si_2W_{18}O_{66}]^{16-}$ host anion, which was described by Hervé et al.[26,27] However, we employed a different synthetic strategy toward the lanthanide-containing polyanions starting from the sodium salt of the trivacant Keggin polyoxoanion $[A\text{-}\alpha\text{-}SiW_9O_{34}]^{10-}$ ($\{\alpha\text{-}SiW_9\}$) precursor in a 1.0 M NaOAc buffer throughout in order to suppress the hydrolysis of the lanthanide cations and to adjust the pH of the reaction system. It is well-known that self-assembly processes of lanthanide-substituted POMs are highly affected by reaction parameters such as the pH values, counterions, stoichiometry, temperature, etc.[20] Furthermore, the $\{\alpha\text{-}SiW_9\}$ polyoxoanion is easily transformed into Keggin- or Dawson-type polyanions and oligomeric structures in an acidic aqueous solution. A literature survey of POM types emerging from the $\{\alpha\text{-}SiW_9\}$ precursor can be found in Table S1 in the Supporting Information.

The results suggest in their entirety that the $\{\alpha\text{-}SiW_9\}$ moiety preferably forms Dawson-type polyanions by dimerization or gives rise to oligomeric structures connected through tungsten atoms or alkali-metal cations at lower pH values (2.4 < pH < 5.9),[26−31] whereas it is prone to reassembly or isomerization into Keggin-type polyanions at higher pH values (5.0 < pH < 6.3).[35−37] In the present $\{\alpha\text{-}SiW_9\}/Ln^{III}$ systems, the transformation from $[\alpha\text{-}SiW_9O_{34}]^{10-}$ to $[\alpha\text{-}Si_2W_{18}O_{66}]^{16-}$ preferably results in the formation of **Gd-1** and **Gd-2**—**Ho-2** under the given reaction conditions (pH 4.4 and 80 °C). Moreover, the crystal structure of the products is obviously affected by the $\{\alpha\text{-}SiW_9\}/Ln^{III}$ ratio: the polymeric compounds (**Gd-1** to **Gd-2**) could not be obtained upon its change from 1:3 to 1:2 or 1:1. The countercation is another important synthetic parameter factor: when Cs^+ was replaced with NH_4^+, Na^+, K^+, or Rb^+, crystals of sufficient quality for single-crystal X-ray diffraction were difficult to obtain. This may be due to electrostatically superior linker qualities of the larger Cs^+ in connection with the $[Ln_2(H_2O)_7Si_2W_{18}O_{66}]^{10-}$ [Ln = Gd^{III} (**Gd-1** and **Gd-2**), Tb^{III}, Ho^{III}] and $[Dy_2(H_2O)_{6.5}(C_2H_4O_2)_{0.5}Si_2W_{18}O_{66}]^{10-}$ polyoxoanions. Most interestingly, **Gd-1** with a 3D inorganic framework structure was obtained from self-assembly reactions in a 1.0 M NaOAc buffer solution by adding a small amount of Cs^+ countercations (0.5 mL of a 1.0 M CsCl solution) to the POM precursor. Continued Cs^+ addition (1.2 mL) led to transformation of the 3D POM framework compound **Gd-1** into the 2D structure of **Gd-2** in solution. In addition, a mixture of **Gd-1** and **Gd-2** in solution could be deliberately produced by adjusting the Cs^+ concentration, which points to an equilibrium between both compounds. Interestingly, this phenomenon was not observed for **Tb-2**, **Dy-2**, or **Ho-2**, so that the solution equilibria of the new compounds are currently under more detailed investigation. Whereas neither alkali-metal cations nor lanthanoid ions bind to the central pocket site of $[Si_2W_{18}O_{66}]^{16-}$, K^+ on this position is obviously essential to maintaining the Wells—Dawson structure of $[\{K(H_2O)_3\}_2\{K(H_2O)_2\}(Si_2W_{18}O_{66})]^{13-}$.[26,27] It goes without saying that the templating role of the cations during POM formation processes cannot be underestimated, as we have, for example, observed for Cs^+ as a stabilizator of the $[Cs\subset Ln_6As_6W_{63}O_{218}(H_2O)_{14}(OH)_4]^{25-}$ (Ln = Eu, Gd, Tb, Dy, Ho, Er) series.[16a] Although Hervé et al. pointed out that dimerization of $[NaSi_2W_{18}O_{66}]^{15-}$ cannot be ruled out, their attempt to study the influence of Na^+ on the reactivity of $[A\text{-}\alpha\text{-}SiW_9O_{34}]^{10-}$ led to the formation of monolacunary $[A\text{-}\alpha\text{-}SiW_{11}O_{39}]^{8-}$, which indicates that the affinity of K^+ for the central position is caused by the size and solubility differences compared to Na^+.

Crystal Structures. Although compounds **Gd-1**, **Tb-2**, **Dy-2**, **Ho-2**, and **Gd-2** have the same dimeric building block in common, the polymeric structure of **Gd-1** differs from the **Gd-2**—**Ho-2** series, as can be seen from the crystallographic data (cf. Table 1). Generally, two lanthanoid cations formally replace

dx.doi.org/10.1021/ic2001943 |*Inorg. Chem.* 2011, 50, 4944–4955

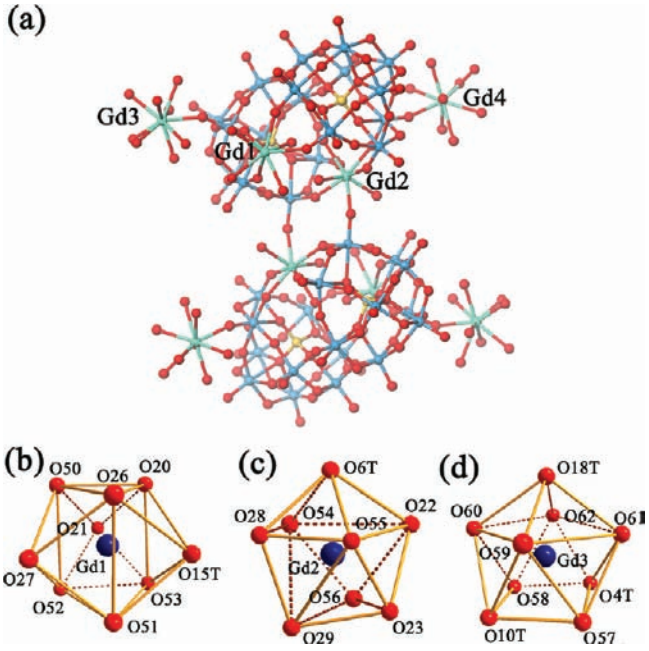

Figure 2. (a) Connectivity of the $\{Gd_2[Gd_2(H_2O)_7Si_2W_{18}O_{66}]\}^{4-}$ anion in **Gd-1** (W, blue; Gd, green; Si, yellow; O, red). Individual Gd geometries of **Gd-1**: (b) tricapped trigonal-prismatic coordination of Gd1; (c) dodecahedral geometry of Gd2; (d) monocapped square-antiprismatic environment of Gd3.

the potassium cations on the exterior pocket sites of the open Wells–Dawson parent type[26] $[\{K(H_2O)_3\}_2\{K(H_2O)_2\}(Si_2W_{18}O_{66})]^{13-}$. The remaining lanthanoid cations are external linkers, thus leading to the formation of 3D networks (**Gd-1**) or 2D polymeric sheetlike materials (**Gd-2**, **Tb-2**, **Dy-2**, and **Ho-2**).

The solid-state structure of **Gd-1** (Figures 2 and 3) consists of the association of one Wells–Dawson anion A-α-$[Si_2W_{18}O_{66}]^{16-}$ with four Gd^{3+} cations: the Gd1 and Gd2 cations are located in the peripheral pocket of the α-$[Si_2W_{18}O_{66}]^{16-}$ anion, whereas the Gd3 and Gd4 cations occupying the α-$[Si_2W_{18}O_{66}]^{16-}$ moiety are bound to the terminal oxygen atoms of the tungsten caps contributed by the monomeric $[A\text{-}\alpha\text{-}SiW_9O_{34}]^{10-}$ precursor. The Gd–Gd distance is 6.338(2) Å in the dimeric Wells–Dawson anion $[Gd_2(H_2O)_7Si_2W_{18}O_{66}]^{10-}$ of **Gd-1**. The Gd1 cation is bound to four terminal oxygen atoms (O20, O21, O26, and O27) from pairs of edge-sharing WO_6 octahedra of the α-$[Si_2W_{18}O_{66}]^{16-}$ framework [Gd1–O distance range: 2.372(9)–2.538(9) Å], to four terminal water ligands (O50, O51, O52, and O53) [Gd1–O distances: 2.438(11)–2.475(11) Å], and to a terminal oxygen atom (O15T′, symmetry code $1-x, y, 0.5-z$) from another neighboring $[Gd_2(H_2O)_7Si_2W_{18}O_{66}]^{10-}$ moiety [Gd1–O15T′: 2.494(10) Å]. The Gd2 cation is also bound to four terminal oxygen atoms (O22, O23, O28, and O29) from pairs of edge-sharing WO_6 octahedra [Gd2–O distances: 2.338(9)–2.418(10) Å] and to three water molecules [O54, O55, and O56 with Gd2–O ranging from 2.405(13) to 2.456(10) Å]. Gd2 is, furthermore, connected to a terminal oxygen atom (O6T′; symmetry code $1-x, -y, -z$) from a neighboring polyanion [Gd2–O6T′: 2.407(9) Å] via symmetry-related Gd–O–W bonds (Gd2–O6T′–W6′ and Gd2′–O6T–W6), with an inversion center displaying a head-on coordination motif including four metal atoms in the dimeric entity $[Gd_2(H_2O)_7Si_2W_{18}O_{66}]^{10-}$ (Figure 2a).

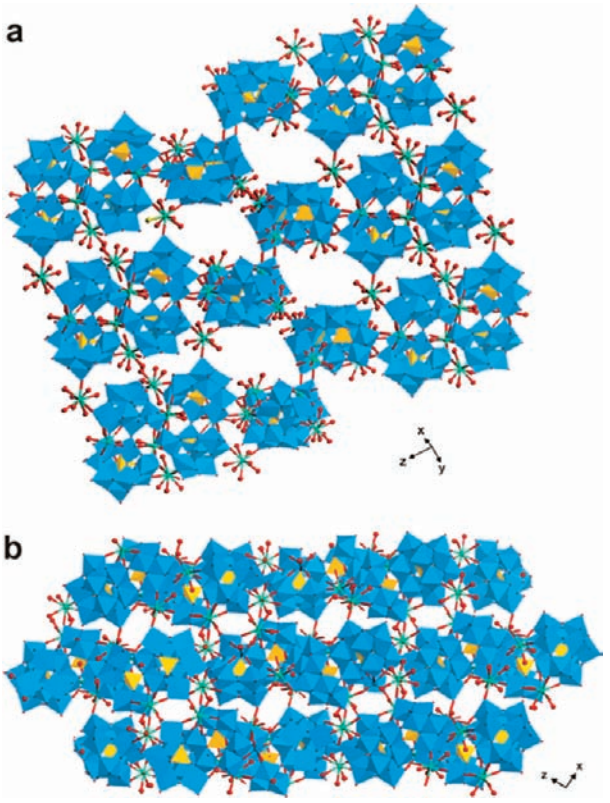

Figure 3. Packing motif of the **Gd-1** type. The cations and crystal water molecules are omitted for clarity (W, blue octahedra; O, red; Si, yellow; Ln, green): (a) polyhedral view of the 3D open framework with 1D channels in **Gd-1**; (b) projection along the *y* axis.

In contrast, the Gd1 cation of the dimer is coordinated to the terminal oxygen atom of W15, thus connecting six metal centers into a hexameric arrangement with inversion symmetry. Of the two Gd3 and Gd4 cations coordinated to the terminal oxygen atoms of the dimeric polyanion $[Gd_2(H_2O)_7Si_2W_{18}O_{66}]^{10-}$, Gd3 is coordinated to W4, W10 $(1-x, y, 0.5-z)$, and W18 $(0.5+x, 0.5+y, z)$ and vice versa via μ-oxo bonds [Gd3–O: 2.366(10)–2.422(9) Å]. Gd4 is coordinated to W1 $(0.5-x, 0.5-y, -z)$ and W12 of the open Wells–Dawson anion via μ-oxo bonds [Gd4–O1T′, 2.319(11) Å; Gd4–O12T, 2.316(10) Å], again in a symmetry-related fashion with an inversion center. The Gd3 coordination sphere is completed by six water molecules, whereas the Gd4 environment is occupied by seven water molecules. While Gd1, Gd2, and Gd4 are coordinated to two polyanions, Gd3 displays the highest degree of connectivity, being attached to three clusters. Therefore, each dimeric cluster $[Gd_2(H_2O)_7Si_2W_{18}O_{66}]^{10-}$ is further linked into a 3D polymeric material via four gadolinium cations (cf. Figure 3). It is noteworthy that this connection mode results in the formation of 1D channels with incorporated crystal water molecules and alkali-metal cations. The cross section of the channels is about 12.7×7.1 Å^2.

From the topological point of view, –Gd1– and –Gd2– can be assigned as the bridging connectors between two $[Gd_2(H_2O)_7Si_2W_{18}O_{66}]^{10-}$ clusters. Consequently, $[Gd_2(H_2O)_7Si_2W_{18}O_{66}]^{10-}$ clusters, Gd3 and Gd4, can be considered as the nodes. In this stylized manner, $[Gd_2(H_2O)_7Si_2W_{18}O_{66}]^{10-}$ moieties are 7-connecting nodes, Gd3 atoms are 3-connecting nodes, and Gd4 atoms are 2-connecting nodes. Therefore, the

dx.doi.org/10.1021/ic2001943 |*Inorg. Chem.* 2011, 50, 4944–4955

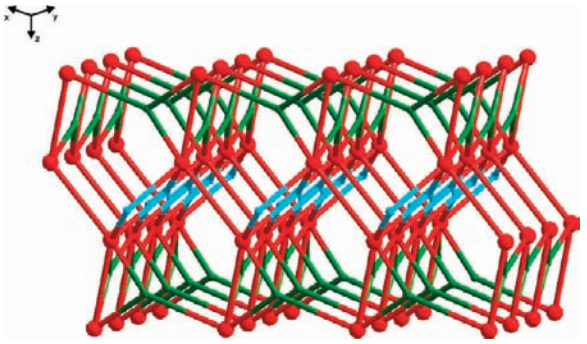

Figure 4. View of the topology of **Gd-1** (red nodes, $[Gd_2(H_2O)_7Si_2W_{18}O_{66}]^{10-}$ clusters; green nodes, Gd3 atoms; blue nodes, Gd4 atoms).

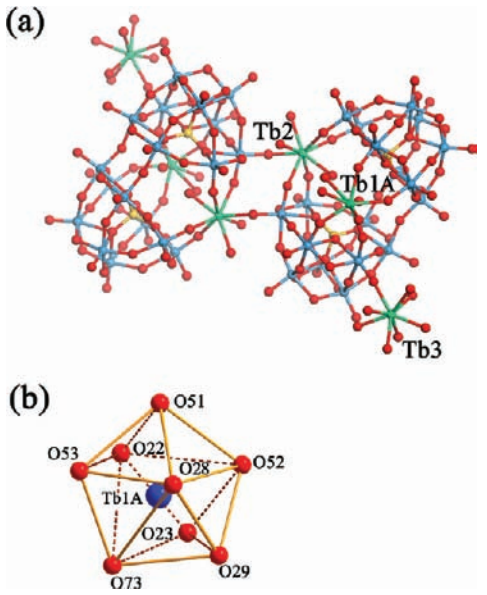

Figure 5. (a) Ball-and-stick representation of the $\{Tb[Tb_2(H_2O)_7Si_2W_{18}O_{66}]\}^{7-}$ anion in **Tb-2** (W, blue; Tb, green; Si, yellow; O, red). (b) Dodecahedral coordination environment of Tb1A in **Tb-2**. Only the major position of the disordered Tb1 (Tb1A) is shown for clarity.

3D framework can be described as a 3,7-connecting network with the Schläfli symbol $[(3.6^2)(3^2.6^8.7^2.8^4.9^5$; Figure 4]. To the best of our knowledge, **Gd-1** represents the first 3D inorganic coordination polymer based on lanthanoid-substituted Wells–Dawson POMs, and the topology of this framework has never been observed in POM chemistry before.

Gd-2, **Tb-2**, **Dy-2**, and **Ho-2** all have the triclinic space group $P\bar{1}$ in common, and their molecular structures are composed of one Wells–Dawson anion A-α-$[Si_2W_{18}O_{66}]^{16-}$ and three crystallographically different lanthanoid cations (Ln = Tb, Dy, Ho, Gd). Because the four compounds are isomorphous, the structure of **Tb-2** is described in detail as a representative example. In the **Tb-2** polyanions, the Tb1 and Tb2 cations occupy the pocket positions of the $[Si_2W_{18}O_{66}]^{16-}$ host anion with a Tb–Tb distance of 6.265(2) Å (Figure 5a). The Tb1A cation is bound to four terminal oxygen atoms (O22, O23, O28, and O29) from pairs of edge-sharing WO_6 octahedra of the α-$[Si_2W_{18}O_{66}]^{16-}$ framework [Tb1A–O distances: 2.317(11)–2.411(10) Å] and to four terminal water ligands [O51, O52, O53, and O73; Tb1A–O distances between 2.36(2) and 2.459(14) Å].

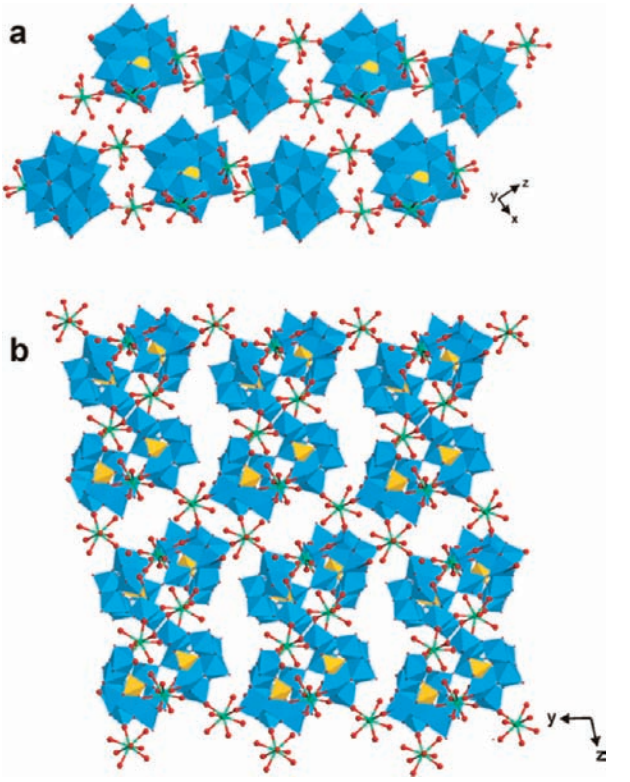

Figure 6. Packing motif of the **Tb-2** type. The cations and crystal water molecules are omitted for clarity (W, blue; O, red; Si, yellow; Ln, green): (a) polyhedral view of 1D chains in the *xz* plane; (b) 2D sheet projection along the *x* axis.

The Tb2 cation, on the other hand, is not only attached to four terminal oxygen atoms (O20, O21, O26, and O27) from the α-$[Si_2W_{18}O_{66}]^{16-}$ framework [Tb2–O distances: 2.292(10)–2.398(10) Å] and three terminal water ligands [O49, O50, and O69; Tb2–O distances between 2.387(11) and 2.472(12) Å] but also bridged to another single polyanion, which is connected to the adjacent cluster via symmetry-related Tb–O–W bonds [Tb2–O6T′–W6′ and Tb2′–O6T–W6; the symmetry code of O6T′, W6′, and Tb2′ is $1-x, -y, 2-z$ with a Tb2–O6T′ distance of 2.341(9) Å], thereby forming a similar head-on species of four metal centers via an inversion center, as has been observed in **Gd-1** (Figure 5a).

The Tb3 cations are coordinated to three terminal oxygen atoms, O4T, O18T′ (symmetry code $x, 1+y, z$), and O17T′ (symmetry code $-x, -y, 1-z$), of the dimeric $[Tb_2(H_2O)_7Si_2W_{18}O_{66}]^{10-}$ polyanions [Tb3–O: 2.321(11)–2.371(10) Å] and to five water molecules [O55–O59 with Tb3–O distances ranging from 2.383(13) to 2.425(12) Å]. Tb3 is attached to three clusters through W4, W18 ($x, 1+y, z$), and W17 ($-x, -y, 1-z$) via μ-oxo bridges, thus connecting the 1D polyanion chains into a 2D sheetlike polymeric material with voids for alkali-metal cations and crystal water molecules (Figure 6).

From the topological point of view, the $[Tb_2(H_2O)_7Si_2W_{18}O_{66}]^{10-}$ clusters represent 4-connecting nodes, the Tb2 atoms can be assigned as bridging connector ligands between two clusters, and the Tb3 atoms are also representing 3-connecting nodes (Figure 7). Therefore, the Schläfli symbol for this 3,4-connected binodal network is $(4^2.6)(4^2.6^2.8^2)$. Moreover, it should be noted that there are some slight structural differences

dx.doi.org/10.1021/ic2001943 |*Inorg. Chem.* 2011, 50, 4944–4955

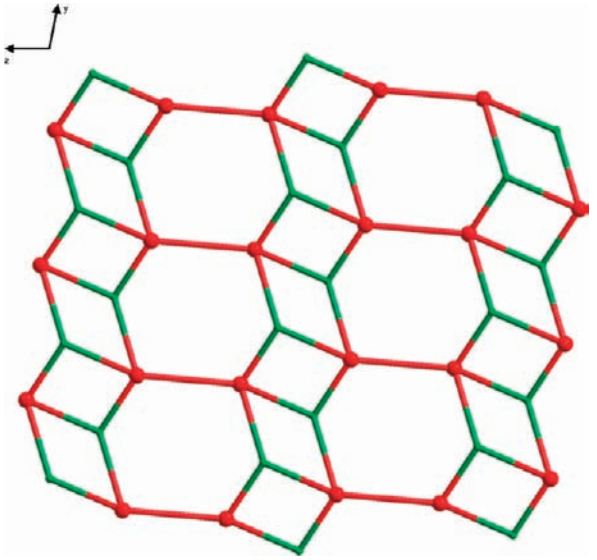

Figure 7. Topological view of **Tb-2** along the *x* axis (red nodes, $[Tb_2(H_2O)_7Si_2W_{18}O_{66}]^{10-}$ clusters; green nodes, Tb3 atoms).

among **Tb-2**, **Dy-2**, **Ho-2**, and **Gd-2**: whereas a half-occupied acetate oxygen and a half-occupied water molecule are bound to the Dy1 ion in **Dy-2**, the analogous bonding sites of the Ln1 ions in **Tb-2** and **Ho-2** are occupied by one terminal water molecule (Figure 1). Furthermore, the Ln^{III} cations in **Tb-2**, **Dy-2**, and **Ho-2** are eight-coordinate, with an almost undistorted dodecahedral coordination environment (Figure 5). In **Gd-2**, the Gd1 and Gd2 cations, located in the external pocket of the α-$[Si_2W_{18}O_{66}]^{16-}$ anion, are eight-coordinate, with a nearly ideal dodecahedral coordination and a distorted square-antiprismatic coordination, respectively. Gd3 is nine-coordinate, adopting a distorted nine-coordinated monocapped square antiprism, with three terminal oxygen atoms from three neighboring $[Gd_2(H_2O)_7Si_2W_{18}O_{66}]^{10-}$ polyanions and four terminal water molecules. The remaining two coordination sites are occupied by two oxygen atoms of the bidentate acetate ligand (cf. Figure 8 and discussion below). All polyanions are arranged as "inversion pairs" in analogy to K_{16}-α-$[Si_2W_{18}O_{66}]$.[22] However, the lanthanoid cations occupy the exterior pockets of the open Wells−Dawson α-$[Si_2W_{18}O_{66}]^{16-}$ anion, and they act as external linkers, thereby differing from the role of K^+ in previous structures and leading to the formation of novel polymeric motifs.

It is noteworthy that the trivalent lanthanoid ions usually exhibit variable higher coordination numbers: eight (dodecahedral, square antiprismatic, or bicapped trigonal prismatic) and nine (tricapped trigonal prismatic or monocapped square antiprismatic).[38] Coordination environments of comparable extension have also been described for cerium-containing polyoxotungstates, such as those for $\{Ce_{16}W_{148}\}$ with two, five, or no aqua ligands per cerium atom[17] and those for $\{Ce_{20}W_{100}\}$ with one or two aqua ligands.[18] The same trend applies for our recently reported gadolinium-containing polyoxotungstate $\{Gd_8W_{124}\}$.[16b] The lanthanoid ions in the present series (**Gd-1**−**Ho-2**) exhibit four different coordination geometries with three to seven terminal aqua ligands, respectively. Concerning **Gd-1**, the coordination polyhedron of Gd1 can be described as a nine-coordinated tricapped trigonal prism (D_{3h}), with the capping oxygen atoms located in the center of three rectangular faces (Figure 2b). The trigonal faces of the tricapped trigonal prism are

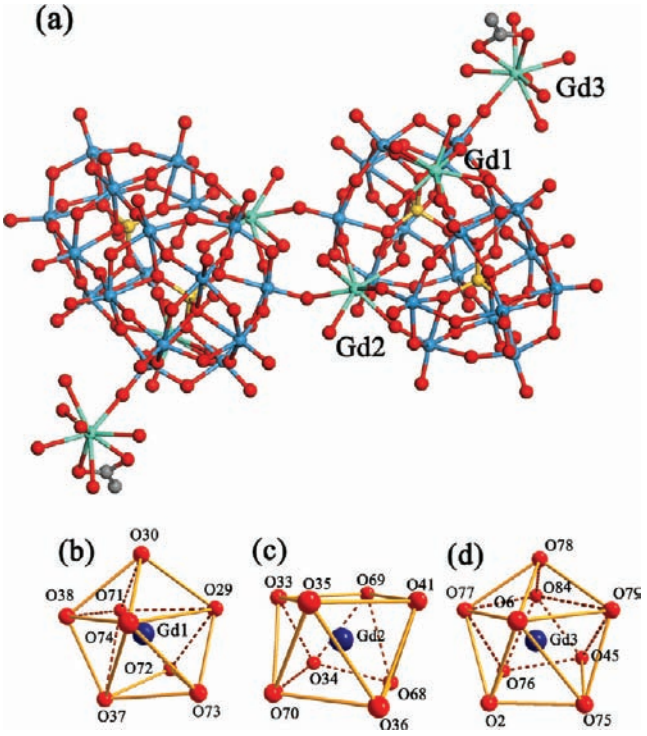

Figure 8. (a) Ball-and-stick representation of the $Gd[Gd_2(H_2O)_7Si_2W_{18}O_{66}]\}^{7-}$ anion in **Gd-2** (W, blue; Tb, green; Si, yellow; O, red; C, gray). Individual Gd geometries of **Gd-2**: (b) dodecahedral coordination environment of Gd1; (c) square-antiprismatic geometry of Gd2; (d) monocapped square-antiprismatic environment of Gd3 in **Gd-2**.

defined by O50−O26−O20 and O52−O51−O53, with O50 eclipsing O52, O26 eclipsing O51, and O20 eclipsing O53. Three oxygen atoms (O21, O27, and O15T) as the three capping atoms of the rectangular faces are approximately trigonal coplanar, with an average angle between capping oxygen atoms and Gd1 of 119.9(2)°, in comparison to 120° for an ideal tricapped trigonal prism. The dihedral angles between the plane defined by the capping atoms and Gd1 and the two trigonal planes are 1.0(4)° and 0.9(3)°, respectively, and the dihedral angle between the two trigonal planes is 1.5(4)°, thereby rendering the overall geometry close to an ideal tricapped trigonal prism.[39] Bond angles between Gd1 and two eclipsing oxygen atoms of opposite trigonal planes are 90.8(4)° for O50−Gd1−O52, 90.7(4)° for O26−Gd1−O51, and 92.6(4)° for O20−Gd1−O53. The coordination geometry around Gd2 is best described as an eight-coordinated dodecahedron (Figure 2c) with an idealized D_{2d} symmetry based on the visualization of two interpenetrating trapezoids that are orthogonal to each other.[40] In the case of Gd2, these trapezoids are defined as the near-planar arrangements of O54−O56−O55−O6T and O22−O23−O29−O28 with average deviations from their least-squares planes of 0.7938 and 0.0212 Å, respectively. The dihedral angle between the two trapezoids is found to be 89.4(2)°. The coordination geometries of both Gd3 and Gd4 are quite close to monocapped square antiprisms with idealized C_{4v} symmetry. In the case of Gd3, for example (Figure 2d), the two approximately antiparallel squares are constituted of O61−O62−O60−O59 and O58−O4T−O57−O10T with a dihedral angle of 2.9(3)°.[41] The capping atom (O18T) is located above the open square plane of O61−O62−O60−O59. The according base diagonals are 3.693(2) and 4.113(2) Å for O4T−O10T and O57−O58,

dx.doi.org/10.1021/ic2001943 |*Inorg. Chem.* 2011, 50, 4944–4955

respectively. They are somewhat different owing to the longer distances of 3.012(2) Å for O57−O10T and 2.712(2) Å for O4T−O57, compared to the other two distances in the square, 2.640(2) and 2.703(2) Å for O4T−O58 and O58−O10T, respectively.

Although both Gd1 and Gd2 in **Gd-2** are eight-coordinate, their local geometries can be differentiated into an almost ideal dodecahedron (D_{2d}) and a slightly distorted square antiprism (D_{4d}), respectively (Figure 8b,d). In the case of the Gd1 cation, two body diagonals of the trapezoids are defined as O74−O73−O72−O71 and O38−O37−O29−O30. The dihedral angle between the trapezoids is 88.8(2)°. In the case of Gd2, two groups of oxygen atoms, namely, (O33, O35, O41, and O69) and (O34, O70, O36, and O68), constitute the two bottom planes of a square antiprism, and the average deviations from their least-squares planes are 0.1119 and 0.1096 Å, respectively. The dihedral angle for the two bottom planes is 5.1(2)°. The Gd3 cation is located in a distorted monocapped square antiprism (Figure 8c), with O78 from one acetate ligand in the capping position. The two antiparallel squares are constituted of O77−O6−O79−O84 and O76−O2−O75−O45, with average deviations of 0.2410 and 0.1527 Å, respectively. The dihedral angle between the two bottom squares is 6.2(3)°. For **Tb-2**, **Dy-2**, and **Ho-2**, the coordination environment of all of the lanthanoids can be described as an almost undistorted eight-coordinated dodecahedron (D_{2d}). Figure 5b displays a near-perfect dodecahedral coordination geometry around the Tb1 cation as a representative example, with the dihedral angle between the two trapezoids being 88.9(2)°. These results show that larger lanthanoids prefer higher coordination numbers and display more flexible coordination geometries compared to smaller lanthanoids: the electrostatic stability of the crystal structure decreases with the lanthanoid radius because of the increasing ligand repulsion in the coordination sphere.[42]

Bond-valence-sum calculations[43] revealed that the valencies of all metal and oxygen atoms within the polyanions $[Ln_2(H_2O)_7Si_2W_{18}O_{66}]_n^{10n-}$ [Ln = Gd^{III} (**Gd-1** and **Gd-2**), Tb^{III}, Ho^{III}] and $[Dy_2(H_2O)_{6.5}(C_2H_4O_2)_{0.5}Si_2W_{18}O_{66}]_n^{10n-}$ are in agreement with their intracluster bonds so that none of the oxygen atoms of the dimeric {α-$Si_2W_{18}O_{66}$} moiety is protonated. Seven or 6.5 terminal aqua ligands, respectively, are coordinated to two of the lanthanoid ions located in the external pocket of the open Wells−Dawson anion {α-$Si_2W_{18}O_{66}$}. This sums up to a net charge of 10− for the above-mentioned polyanions, which is compensated for by their countercations in the solid state. However, to balance the charge, we added two protons in **Tb-2**, one proton in **Dy-2**, and two protons in **Gd-2**, respectively, as the products were isolated from an acidic aqueous solution (pH 4.4). These protons cannot be located crystallographically and are assumed to be delocalized over the entire structure, which is a commonly observed phenomenon in the chemistry of POMs.[44] Moreover, the average Ln−O distances in all of the compounds tentatively indicate the presence of a lanthanoid contraction effect with 2.42(2) Å for **Gd-1**, 2.41(1) Å for **Gd-2**, 2.39(3) Å for **Tb-2**, 2.36(2) Å for **Dy-2**, and 2.34(2) Å for **Ho-2**.

FT-IR Spectroscopy. The FT-IR spectra of all compounds (**Gd-1** and **Gd-2**, **Tb-2**, **Dy-2**, and **Ho-2**) display related characteristic ν_{as}(Si−O_a), terminal ν_{as}(W−O_t), corner-sharing ν_{as}(W−O_b), and edge-sharing ν_{as}(W−O_c) asymmetrical vibration peaks due to the presence of the common open Wells−Dawson anion A-α-$[Si_2W_{18}O_{66}]^{16-}$ (cf. Figure S1 in the Supporting Information).[1] In the IR spectrum of **Gd-1**, the peak at 1001 cm^{-1} can be attributed to ν_{as}(Si−O_a) and the characteristic bands at 938, 871, 833, 808, and 723 cm^{-1} are assigned to ν_{as}(W−O_t), ν_{as}(W−O_b), and ν_{as}(W−O_c). The characteristic features in the IR spectrum of **Gd-2** at 1002, 934, 886, 814, and 720 cm^{-1} arise from ν_{as}(Si−O_a), ν_{as}(W═O_d), ν_{as}(W−O_b), and ν_{as}(W−O_c), respectively. The peaks in the IR spectrum of **Tb-2** at 1002, 937, 876, 818, and 718 cm^{-1} can be assigned to ν_{as}(Si−O_a), ν_{as}(W═O_d), ν_{as}(W−O_b), and ν_{as}(W−O_c). In the IR spectrum of **Dy-2**, the peaks at 1002, 940, 882, 817, and 716 cm^{-1} are attributed as follows: ν_{as}(Si−O_a), ν_{as}(W═O_d), ν_{as}(W−O_b), and ν_{as}(W−O_c). Likewise, the characteristic vibrations in the IR spectrum of **Ho-2** at 1003, 939, 868, 833, 809, and 714 cm^{-1} arise from ν_{as}(Si−O_a), ν_{as}(W═O_d), ν_{as}(W−O_b), and ν_{as}(W−O_c). Moreover, the gradual blue shift of the ν_{as}(W−O_c) vibration points to the influence of the lanthanoid contraction on the FT-IR spectra.

UV/Vis Spectroscopy. UV/vis spectra of **Gd-1** and **Gd-2**, **Tb-2**, **Dy-2**, and **Ho-2** were recorded in an aqueous solution in the 600−190 nm range (cf. Figure S2 in the Supporting Information). The UV spectra of **Gd-1** and **Tb-2** have two characteristic absorption bands at 202−205 and 250 nm in common. The absorption band at higher energies can be ascribed to the p_π−d_π charge-transfer transitions of the O_t → W bonds, whereas the latter low-energy absorption band is due to the p_π−d_π charge-transfer transitions of the $O_{b(c)}$ → W bonds. However, the UV spectra of **Gd-2**, **Dy-2**, and **Ho-2** display only the higher-energy absorption band centered at 194−200 nm that can be assigned to the p_π−d_π charge-transfer transitions of the O_t → W bonds.[45a] The blue shift of the absorption bands at higher energies might reflect the influence of the different lanthanide cations on the local geometry of the dimeric $[Ln_2(H_2O)_7Si_2W_{18}O_{66}]^{10-}$ (Ln = Gd, Ho, Tb) and $[Dy_2(H_2O)_{6.5}(C_2H_4O_2)_{0.5}Si_2W_{18}O_{66}]^{10-}$ polyanions. Similar phenomena had already been reported in previous related studies on the reaction of lanthanide cations with monovacant Keggin polyoxotungstates.[45] However, we did not observe the absorption bands of the trivalent lanthanides in an aqueous solution, which may be due to concealment by the strong (O → W) charge-transfer bands. Therefore, we also recorded the solid-state absorption spectra of all samples in the 400−850 nm range. For **Tb-2**, two weak absorption bands around 466 and 498 nm correspond to the $^7F_6$ → $^5D_3$ and $^7F_6$ → $^5D_4$ transitions of the Tb^{3+} ion (cf. Figure S3 in the Supporting Information). Three weak absorption bands appear in the visible range for **Dy-2** at 428, 453, and 475 nm, and they are assigned to the $^6H_{15/2}$ → $^4F_{9/2}$, $^6H_{15/2}$ → $^4I_{15/2}$, $^6H_{15/2}$ → $^4G_{11/2}$ transitions of Dy^{3+}. Two stronger bands at 757 and 806 nm in the near-IR region indicate the $^6H_{15/2}$ → $^6F_{3/2}$ and $^6H_{15/2}$ → $^6F_{5/2}$ transitions of the Dy^{3+} ion, respectively (cf. Figure S4 in the Supporting Information).[46] For **Ho-2**, seven absorption bands around 418, 451, 468, 474, 486, 537, and 642 nm can be assigned to the $^5I_8$ → $^5G_5$, $^5I_8$ → ($^5F_1$, $^5G_6$), $^5I_8$ → $^3K_8$, $^5I_8$ → $^5F_2$, $^5I_8$ → $^5F_3$, $^5I_8$ → ($^5F_4$, $^5S_2$), and $^5I_8$ → $^5F_5$ transitions of the Ho^{3+} ion (Figure 9), but only the $^5I_8$ → ($^5F_1$, $^5G_6$) and $^5I_8$ → ($^5F_4$, $^5S_2$) transitions notably contribute to the color of this compound.[47] Interestingly, there is a rapid color change between light yellow and pink when the **Ho-2** sample is illuminated with incandescent light or daylight because of the light-source-dependent color of the Ho^{3+} centers.[46] This is a promising feature for the preparation of photochromic inorganic materials.[47]

PXRD Characterization. The phase purity of representative **Gd-1** and **Gd-2**, **Tb-2**, **Dy-2**, and **Ho-2** samples was checked by

dx.doi.org/10.1021/ic2001943 |*Inorg. Chem.* 2011, 50, 4944–4955

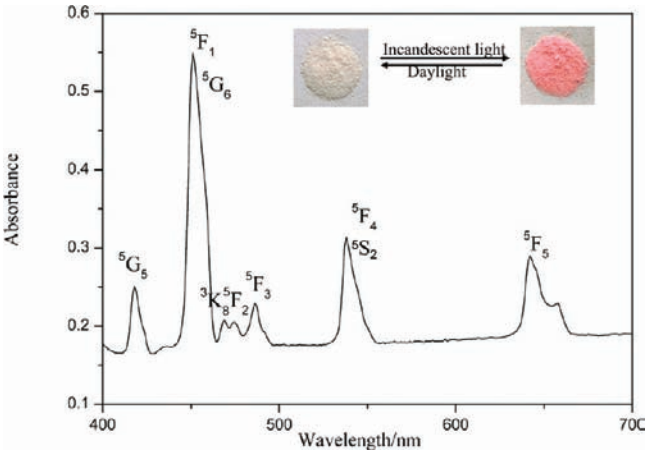

Figure 9. Solid-state UV/vis spectra of **Ho-2** measured in the 300−700 nm range. Inset: color change of **Ho-2** upon irradiation from different light sources.

bulk PXRD measurements (Figures S10−S14 in the Supporting Information). The PXRD patterns for the **Gd-2**−**Ho-2** series are quite similar, indicating the isostructural character of the four compounds. The experimental diffraction patterns are in line with the calculated data, thus confirming the results of single-crystal X-ray structure determination.

Photoluminescence Spectroscopy. In order to investigate the photoluminescence behavior of **Gd-1** and **Gd-2**, **Tb-2**, **Dy-2**, and **Ho-2**, their spectra were recorded at room temperature upon photoexcitation. Only **Tb-2** and **Dy-2** exhibit millisecond-order luminescence lifetimes that could be measured under the given conditions (Figure 10). The terbium compound **Tb-2** exhibited green photoluminescence under excitation at 255 nm. The emission spectrum displays four characteristic emission peaks of Tb^{3+} at 487, 532, 579, and 624 nm, which can be assigned to transition of the $^5D_4$ excited state to the corresponding ground state ^7F_J (J = 6, 5, 4, 3) of the Tb^{3+} ion.[48] The $^5D_4 \rightarrow {}^7F_6$ transition is a magnetic-dipole transition, and its intensity varies with the strength of the ligand field experienced by the Tb^{3+} ion. The emission to magnetic-dipole transition ($^5D_4 \rightarrow {}^7F_6$) in **Tb-2** does not show splitting, which is in agreement with the results of the crystal structure determination that indicate closely related coordination environments for the terbium ions. The strongest emission band $^5D_4 \rightarrow {}^7F_5$ is an electric-dipole transition that is exceptionally sensitive to changes in the chemical bonds in the vicinity of the Tb^{3+} ion. The intensity of the $^5D_4 \rightarrow {}^7F_5$ transition increases with a decrease in the site symmetry of the Tb^{3+} ion. Therefore, the intensity ratio of the $I(^5D_4 \rightarrow {}^7F_5)$ to $I(^5D_4 \rightarrow {}^7F_6)$ transitions is frequently used to quantify the coordination state and site symmetry of the rare-earth ions.[48] In the present case, the intensity ratio $I(^5D_4 \rightarrow {}^7F_5)$ to $I(^5D_4 \rightarrow {}^7F_6)$ is about 3.1, which further confirms the closely related low-symmetry coordination environments of the three Tb^{3+} ions. The dysprosium-containing POM **Dy-2** displays two characteristic $^4F_{9/2} \rightarrow {}^6H_{15/2}$ and $^4F_{9/2} \rightarrow {}^6H_{13/2}$ transitions upon excitation at 350 nm, leading to blue (around 479 nm) and yellow (around 574 nm) emission, respectively.[49] The $^4F_{9/2} \rightarrow {}^6H_{13/2}$ transition is assigned to a hypersensitive transition with ΔJ = 2, which is strongly influenced by the chemical environment of Dy^{3+}. Generally, the low intensity of the luminescence of the Dy^{3+} ion in complexes can be explained in terms of effective radiationless

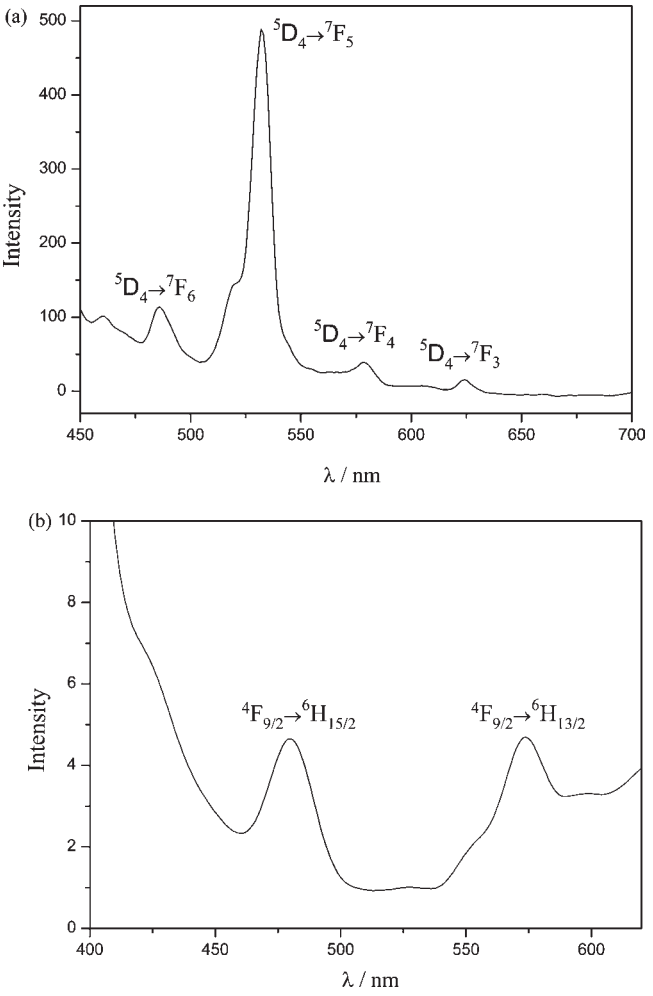

Figure 10. Photoluminescence spectra of **Tb-2** (a) and **Dy-2** (b) at room temperature (excitation wavelengths at 255 and 350 nm).

deactivation in the excited state due to the small energy gap between the excited level $^4F_{9/2}$ and the sublevels of the ground-state terms $^6H_{3/2}$, $^6H_{5/2}$, and $^6H_{5/2}$.[50]

Magnetic Properties. The magnetic susceptibility of **Gd-1** and **Gd-2** was investigated with respect to the magnetic Gd^{3+} centers. Plots of the molar magnetic susceptibility χ_m per gadolinium ion and $1/\chi_m$ vs T in the range between 2 and 300 K for an applied magnetic field of 2000 Oe are shown in Figure 11. Both **Gd-1** and **Gd-2** display characteristic paramagnetic behavior over the entire temperature range, and the experimental data fit well to a Curie law ($\chi = C/T$) with the respective Curie constants of $C_{\mathbf{Gd\text{-}1}}$ = 8.00 emu K Oe^{-1} mol^{-1} and $C_{\mathbf{Gd\text{-}2}}$ = 8.20 K Oe^{-1} mol^{-1}. Likewise, the $1/\chi_m$ vs T curves are almost perfectly linear. The effective magnetic moments μ_{eff} per gadolinium ion [$\mu_{eff}^2 = 3Ck/\mu_B^2N$ (k = Boltzmann's constant, μ_B = Bohr magneton, and N = Avogadro's number)] were derived from the Curie constant. The obtained values of 8.03 μ_B for **Gd-1** and 8.13 μ_B for **Gd-2** are close to the expected spin-only value (μ_{eff} = 7.94 μ_B) for the free Gd^{3+} ion. Furthermore, the refined spin values S for **Gd-1** and **Gd-2** were determined as 3.54 and 3.58, respectively, which agrees well with the spin of noninteracting gadolinium centers ($S = {}^7/_2$). These results also indicate that a spin−spin coupling through O−W−O bridges is negligible because of large Gd−Gd distances in both **Gd-1** and

dx.doi.org/10.1021/ic2001943 |*Inorg. Chem.* 2011, 50, 4944–4955

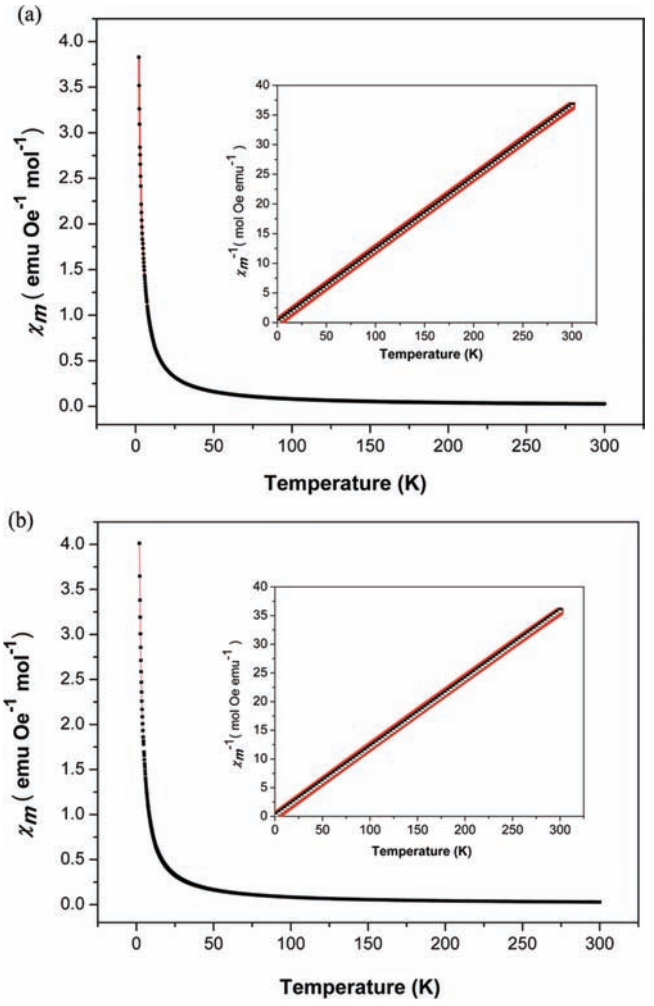

Figure 11. Temperature dependence of the magnetic susceptibility χ_m and χ_m^{-1} (inset) from 2 to 300 K for (a) **Gd-1** and (b) **Gd-2**.

Gd-2. We observed related phenomena in our previous studies on other gadolinium-containing POMs.[16]

Electrochemistry. In order to electrochemically characterize compounds **Gd-1** and **Gd-2**−**Ho-2**, we carried out CV measurements in a sodium acetate buffer (pH 4.4) solution as the supporting electrolyte (Figure 12). The results indicate that all compounds show almost identical CV behavior, which is probably because of the common presence of the Wells−Dawson anion A-α-$[Si_2W_{18}O_{66}]^{16-}$ in their structures. For example, the reduction waves of **Gd-1** occur at −0.657 V (E_{pc1}) and −0.901 V (E_{pc2}), respectively, in two separate steps. These waves can be assigned to the reduction of tungsten centers. During the reoxidation process, one oxidation peak E_{pa1} located at −0.562 V is associated with first reduction wave E_{pc1}. The peak potential difference between E_{pa1} and E_{pc1} is 95 mV for this redox couple (I−I′), corresponding to a reversible one-electron-redox process.[51] However, the reoxidation wave associated with the second reduction process is more complex through the splitting of the reoxidation pattern of tungsten waves into two waves located at −0.806 V (E_{pa2}) and −0.682 V (E_{pa3}). Related observations have been encountered in the electrochemical behavior of dilacunary $[\gamma\text{-}SiW_{10}O_{36}]^{8-}$ and the transition-metal-substituted decatungstosilicate $[M(H_2O)_2(\gamma\text{-}Si_2W_{20}O_{70})]^{10-}$ (M = Mn^{2+}, Co^{2+}, Ni^{2+}).[31,32] These results might indicate that a

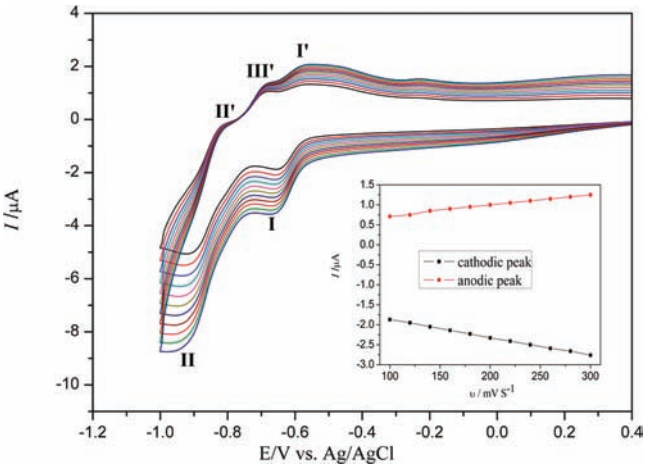

Figure 12. Cyclic voltammograms of 0.2 mM **Gd-1** in a pH 4.4 (1.0 M CH_3COONa/CH_3COOH) buffer at different scan rates (from inner to outer plots: 100, 120, 140, 160, 180, 200, 220, 240, 260, and 300 mV s^{-1}). Inset: plots of the anodic and cathodic peak currents of I−I′ against the scan rates.

strong irreversible electron-transfer process takes place in the second redox step. Furthermore, no redox activity of lanthanide cations was detected over the potential range from −1.0 to +1.0 V, which is in line with studies on the redox processes of lanthanide-substituted Dawson-type arsenotungstates (α_2-$[Ln(As_2W_{17}O_{61})_2]^{17-}$ and $\{[(\alpha_2\text{-}As_2W_{17}O_{61})Ln(H_2O)_2]_2\}^{14-}$).[52] The CV curves of **Gd-1** at different scan rates were also investigated. When the scan rate was changed from 100 to 300 mV s^{-1}, the peak potentials varied gradually: the cathodic peak potentials were shifted toward negative values, whereas the corresponding anodic peak potentials were shifted to the opposite direction with an increase of the scan rate. In addition, the peak currents are proportional to the scan rate (ν), which indicates that the redox process is surface-controlled with a fast exchange rate of electrons. Because the cyclic voltammograms of **Tb-2**, **Dy-2**, **Ho-2**, and **Gd-2** exhibit almost identical CV curves in comparison with **Gd-1** (Figures S6−S9 in the Supporting Information), they are not individually discussed.

TGA. TGA measurements on **Gd-1** and **Gd-2**, **Tb-2**, **Dy-2**, and **Ho-2** were performed under a nitrogen flow in the temperature range from 30 to 800 °C. The TGA curves of all of the compounds (shown in Figure S5 in the Supporting Information) exhibit one weight loss step in the temperature range of 30−300 °C, respectively. The observed weight loss for **Gd-1** is 10.3% (calcd 10.2%), corresponding to the release of crystal water molecules and adsorbed water molecules. The corresponding values are 5.2% (calcd 5.3%) for **Tb-2** and 6.7% (calcd 7.6%) for **Ho-2**. For **Dy-2**, one weight loss step of 7.6% corresponds to the loss of water molecules and 0.5 formula units of the acetate ligand (calcd 7.9%). For **Gd-2**, one weight loss stage of 7.8% (calcd 7.9%) can be assigned to the loss of water molecules and one acetate ligand. The related shapes of the TGA curves, furthermore, underscore the structural similarities of the compounds.

■ CONCLUSIONS

A series of five lanthanoid-containing silicotungstates of the novel $[Ln_2(H_2O)_7Si_2W_{18}O_{66}]^{10-}$ (Ln = Gd, Ho, Tb) and $[Dy_2(H_2O)_{6.5}(C_2H_4O_2)_{0.5}Si_2W_{18}O_{66}]_n^{10n-}$ types were obtained

dx.doi.org/10.1021/ic2001943 |Inorg. Chem. 2011, 50, 4944–4955

from the one-step reaction of the $[A\text{-}\alpha\text{-}SiW_9O_{34}]^{10-}$ precursor with Ln^{III} cations in buffer solutions. All compounds were structurally characterized, and their packing motifs depend on the size of the lanthanoid cation. Whereas the **Gd-1** representative of the new compound family crystallizes in a 3D network structure, **Gd-2** and the remaining compounds consist of 2D polyoxotungstate sheets. This is in line with the special role of Gd^{3+} in our previous studies on large polyoxotungstates, because the novel $\{Gd_8W_{124}\}$ type is exclusively formed with this member of the lanthanoid series.[16b] The individual coordination environments of the lanthanoid cations also differ between the two new 3D and 2D compound types. Both structural motifs display accessible voids that are occupied by alkali-metal cations and crystal water molecules. The influence of the lanthanoid contraction is also evident from the FT-IR spectra, and the newly discovered family of open Wells−Dawson host anions with lanthanoid guests was characterized with a wide range of analytical methods. Their electrochemical properties were studied by CV in a sodium acetate buffer (pH 4.4) as the supporting electrolyte. The **Tb-2** and **Dy-2** compounds exhibit room temperature photoluminescence upon excitation, and the **Ho-2** compound displays photochromic behavior. The magnetic behavior of **Gd-1** and **Gd-2** between 2 and 300 K was found to be paramagnetic and in agreement with the spin of noninteracting gadolinium centers. In conclusion, our work provides new incentives to explore controllable assemblies and structural transformations of Ln-POM-based coordination polymers with distinct structural features and properties.

■ ASSOCIATED CONTENT

Supporting Information. X-ray crystallographic files (in CIF format), product range emerging from the $[A\text{-}\alpha\text{-}SiW_9O_{34}]^{10-}$ precursor, FT-IR spectra, UV/vis spectra, TGA, cyclic voltammograms, and PXRD patterns for compounds **Gd-1**, **Tb-2**, **Dy-2**, **Ho-2**, and **Gd-2**. This material is available free of charge via the Internet at http://pubs.acs.org.

■ AUTHOR INFORMATION

Corresponding Author

*E-mail: greta.patzke@aci.uzh.ch. Tel: +41 44 635 4691. Fax: +41 44 635 6802.

■ ACKNOWLEDGMENT

This work was supported by the Swiss National Science Foundation (SNSF Professorship PP002-114711/1), and financial support from the University of Zurich is gratefully acknowledged. The authors thank Prof. Dr. Markus Niederberger, Dr. Marta D. Rossell, and Niklaus Kränzlin (Laboratory for Multifunctional Materials, Department of Materials, ETH Zurich) for PXRD measurements. L.N. thanks the China Scholarship Council for a Ph.D. research fellowship.

■ REFERENCES

(1) Pope, M. T. *Heteropoly and Isopoly Oxometalates*; Springer: Berlin, 1983.

(2) Pope, M. T.; Müller, A. *Angew. Chem.* **1991**, *103*, 56. *Angew. Chem., Int. Ed.* **1991**, *30*, 34–48.

(3) Pope, M. T. *Compr. Coord. Chem. II* **2003**, *4*, 635–678.

(4) Hill, C. L. *Compr. Coord. Chem. II* **2003**, *4*, 679–759. Hill, C. L.; Prosser-McCartha, C. M. *Coord. Chem. Rev.* **1995**, *143*, 407–455.

(5) Cronin, L. *Compr. Coord. Chem. II* **2003**, *7*, 1–56.

(6) *Polyoxometalate Molecular Science*; Borras-Almenar, J. J., Coronado, E., Müller, A., Pope, M. T., Eds.; Kluwer: Dordrecht, The Netherlands, 2004.

(7) *Polyoxometalates: From Platonic Solids to Antiretroviral Activity*; Pope, M. T., Müller, A., Eds.; Kluwer: Dordrecht, The Netherlands, 1994.

(8) Kortz, U.; Müller, A.; van Slageren, J.; Schnack, J.; Dalal, N. S.; Dressel, M. *Coord. Chem. Rev.* **2009**, *253*, 2315–2320.

(9) Kögerler, P.; Tsukerblat, B.; Müller, A. *Dalton Trans.* **2010**, *39*, 21–36.

(10) Hill, C. L. Ed. *Chem. Rev.* **1998**, *98*, 1−389 (Special Issue on Polyoxometalates).

(11) (a) Hasenknopf, B. *Front. Biosci.* **2005**, *10*, 275–287. (b) Korenev, V. S.; Boulay, A. G.; Dolbecq, A.; Sokolov, M. N.; Hijazi, A.; Floquet, S.; Fedin, V. P.; Cadot, E. *Inorg. Chem.* **2010**, *49*, 9740–9742. (c) Orlandi, M.; Argazzi, R.; Sartorel, A.; Carraro, M.; Scorrano, G.; Bonchio, M.; Scandola, F. *Chem. Commun.* **2010**, *46*, 3152–3154. (d) Yin, Q.; Tan, J. M.; Besson, C.; Geletii, Y. V.; Musaev, D. G.; Kuznetsov, A.; Luo, Z.; Hardcastle, K. I.; Hill, C. L. *Science* **2010**, *328*, 342–345.

(12) *Polyoxometalate Chemistry: From Topology via Self-Assembly to Applications*; Pope, M. T., Müller, A., Eds.; Kluwer: Dordrecht, The Netherlands, 2001.

(13) Katsoulis, D. E. *Chem. Rev.* **1998**, *98*, 359–387.

(14) (a) Howell, R. C.; Perez, F. G.; Jain, S. W.; Horrocks, D., Jr.; Rheingold, A. L.; Francesconi, L. C. *Angew. Chem., Int. Ed.* **2001**, *40*, 4031–4034. (b) Yamase, T.; Naruke, H.; Sasaki, Y. *J. Chem. Soc., Dalton Trans.* **1990**, 1687–1696. (c) Niu, J. Y.; Guo, D. J.; Wang, J. P.; Zhao, J. W. *Cryst. Growth Des.* **2004**, *4*, 241–247. (d) Niu, J. Y.; Wei, M. L.; Wang, J. P.; Dang, D. B. *Eur. J. Inorg. Chem.* **2004**, 160–170. (e) Mialane, P.; Dolbecq, A.; Sécheresse, F. *Chem. Commun.* **2006**, 3477–3485. (f) Zhongfeng, L.; Weisheng, L.; Xiaojing, L.; Fengkui, P.; Yingxia, L.; Hao, L. *Magn. Reson. Imaging* **2007**, *25*, 412–417.

(15) (a) Hussain, F.; Spingler, B.; Conrad, F.; Speldrich, M.; Kögerler, P.; Boskovic, C.; Patzke, G. R. *Dalton Trans.* **2009**, 4223–4225. (b) Hussain, F.; Conrad, F.; Patzke, G. R. *Angew. Chem.* **2009**, *121*, 9252–9255. *Angew. Chem., Int. Ed.* **2009**, *48*, 9088–9091. (c) Hussain, F.; Patzke, G. R. *CrystEngComm* **2011**, *13*, 530–536.

(16) Wassermann, K.; Dickman, M. H.; Pope, M. T. *Angew. Chem.* **1997**, *109*, 1513–1516. *Angew. Chem., Int. Ed.* **1997**, *36*, 1445–1448.

(17) Bassil, B. S.; Dickman, M. H.; Römer, I.; von der Kammer, B.; Kortz, U. *Angew. Chem., Int. Ed.* **2007**, *46*, 6192–6195.

(18) Hussain, F.; Gable, R. W.; Speldrich, M.; Kögerler, P.; Boskovic, C. *Chem. Commun.* **2009**, 328–330.

(19) (a) Pope, M. T. *Handbook on the Physics and Chemistry of Rare Earths*; North-Holland: Amsterdam, The Netherlands, 2007; Vol. 38, pp 337−382. (b) Drewes, D.; Piepenbrink, M.; Krebs, B. *Z. Anorg. Allg. Chem.* **2006**, *632*, 534–536. (c) Li, F.; Xu, L.; Wei, Y.; Gao, G.; Fan, L.; Li, Z. *Inorg. Chim. Acta* **2006**, *359*, 3795–3799. (d) Mialane, P.; Dolbecq, A.; Marrot, J.; Sécheresse, F. *Inorg. Chem. Commun.* **2005**, *8*, 740–742. (e) Fang, X.; Anderson, T.; Benelli, C.; Hill, C. L. *Chem.—Eur. J.* **2005**, *11*, 712–718. (f) Fukaya, K.; Yamase, T. *Angew. Chem., Int. Ed.* **2003**, *42*, 654–658. (g) Xue, G. L.; Vaissermann, J.; Gouzerh, P. *J. Cluster Sci.* **2002**, *13*, 409–421. (h) Cronin, L.; Beugholt, C.; Krickemeyer, E.; Schmidtmann, M.; Bögge, H.; Kögerler, P.; Kim, T.; Luong, K.; Müller, A. *Angew. Chem., Int. Ed.* **2002**, *41*, 2805–2808. (i) Howell, R. C.; Perez, F. G.; Jain, S.; Horrocks, W. D., Jr.; Rheingold, A. L.; Francesconi, L. C. *Angew. Chem., Int. Ed.* **2001**, *40*, 4031–4034. (j) Müller, A.; Beugholt, C.; Bögge, H.; Schmidtmann, M. *Inorg. Chem.* **2000**, *39*, 3112–3113.

(20) Peacock, R. D.; Weakley, T. J. R. *J. Chem. Soc. A* **1971**, 1836–1839.

(21) Sadakane, M.; Dickman, M. H.; Pope, M. T. *Angew. Chem., Int. Ed.* **2000**, *39*, 2914–2916.

(22) Mialane, P.; Lisnard, L.; Mallard, A.; Marrot, J.; Antic-Fidancev, E.; Aschehoug, P.; Vivien, D.; Sécheresse, F. *Inorg. Chem.* **2003**, *42*, 2102–2108.

(23) Bassil, B. S.; Dickman, M. H.; von der Kammer, B.; Kortz, U. *Inorg. Chem.* **2007**, *46*, 2452–2458.
(24) (a) Niu, J. Y.; Zhao, J. W.; Wang, J. P. *Inorg. Chem. Commun.* **2004**, *7*, 876–879. (b) Wang, J. P.; Zhao, J. W.; Niu, J. Y. *Sci. China, Ser. B: Chem.* **2005**, *48*, 343–351. (c) Wang, J. P.; Duan, X. Y.; Du, X. D.; Niu, J. Y. *Cryst. Growth Des.* **2006**, *6*, 2266–2270. (d) Wang, J. P.; Zhao, J. W.; Duan, X. Y.; Niu, J. Y. *Cryst. Growth. Des.* **2006**, *6*, 507–513.
(25) An, H. Y.; Han, Z. B.; Xu, T. Q. *Inorg. Chem.* **2010**, *49*, 11403–11414.
(26) Laronze, N.; Marrot, J.; Hervé, G. *Chem. Commun.* **2003**, 2360–2361.
(27) Laronze, N.; Marrot, J.; Hervé, G. *Inorg. Chem.* **2005**, *44*, 1275–1281.
(28) Laronze, N.; Haouas, M.; Marrot, J.; Taulelle, F.; Hervé, G. *Angew. Chem., Int. Ed.* **2006**, *45*, 145–148.
(29) Laronze, N.; Marrot, J.; Hervé, G. *C. R. Chim.* **2006**, *9*, 1467–1471.
(30) (a) Bi, L.; Kortz, U. *Inorg. Chem.* **2004**, *43*, 7961–7962. (b) Nellutla, S.; Tol, J.; Dalal, N. S.; Bi, L.; Kortz, U.; Keita, B.; Nadjo, L.; Khitrov, G. A.; Marshall, A. G. *Inorg. Chem.* **2005**, *44*, 9795–9806.
(31) Bassil, B. S.; Dickman, M. H.; Reicke, M.; Kortz, U.; Keita, B.; Nadjo, L. *Dalton Trans.* **2006**, 4253–4259.
(32) Tézé, A.; Hervé, G.; Finke, R. G.; Lyon, D. K. *Inorg. Synth.* **1990**, *27*, 85–135.
(33) *CrysAlis Pro*; Oxford Diffraction Ltd.: Abingdon, U.K., 2007.
(34) Sheldrick, G. M. *Acta Crystallogr.* **2008**, *A64*, 112–122.
(35) Liu, J. F.; Ortega, F.; Sethuraman, P.; Katsoulis, D. E.; Costello, C. E.; Pope, M. T. *J. Chem. Soc., Dalton Trans.* **1992**, 1901–1906.
(36) Chatterjee, R.; Ali, M.; Drew, M. G. B.; Nethaji, M.; Mondal, S.; Mukherjee, M. *Transition Met. Chem.* **2009**, *34*, 1–5.
(37) Laronze, N.; Marrot, J.; Hervé, G. *Inorg. Chem.* **2003**, *42*, 5857–5862.
(38) Helm, L.; Merbach, A. E. *Coord. Chem. Rev.* **1999**, *187*, 151–181.
(39) Favas, M. C.; Kepert, D. L. *Prog. Inorg. Chem.* **1981**, *28*, 309–367.
(40) (a) Porai-Koshits, M. A.; Aslanov, L. A. *Zh. Strukt. Khim.* **1972**, *13*, 266–276. (b) Hoard, J. L.; Silverton, J. V. *Inorg. Chem.* **1963**, *2*, 235–243. (c) Kepert, D. L. *J. Chem. Soc.* **1965**, 4736–4744. (d) Lippard, S. J.; Russ, B. J. *Inorg. Chem.* **1968**, *7*, 1686–1688. (e) Muetterties, E. L. *Inorg. Chem.* **1973**, *12*, 1963–1966.
(41) (a) Corbett, J. D. *Struct. Bonding (Berlin)* **1997**, *87*, 157–193. (b) Fässler, T. F.; Hoffmann, R. *Angew. Chem., Int. Ed.* **1999**, *38*, 543–546.
(42) Karraker, D. G. *J. Chem. Educ.* **1970**, *47*, 424–430.
(43) (a) Brown, I. D.; Altermatt, D. *Acta Crystalllogr., Sect. B* **1985**, *41*, 244–247. (b) Trzesowska, A.; Kruszynski, R.; Bartczak, T. J. *Acta Crystallogr., Sect. B* **2004**, *60*, 174–178.
(44) (a) Mialance, P.; Dolbecq, A.; Lisnard, L.; Mallard, A.; Marrot, J.; Sécheresse, F. *Angew. Chem., Int. Ed.* **2002**, *41*, 2398–2401. (b) An, H. Y.; Wang, E. B.; Xiao, D. R.; Li, Y. G.; Su, Z. M.; Xu, L. *Angew. Chem., Int. Ed.* **2006**, *45*, 904–908. (c) Du, D. Y.; Qin, J. S.; Li, S. L.; Lan, Y. Q.; Wang, X. L.; Su, Z. M. *Aust. J. Chem.* **2010**, *63*, 1398–1395.
(45) (a) Niu, J. Y.; Wang, K. H.; Chen, H. N.; Zhao, J. W.; Ma, P. T.; Wang, J. P.; Li, M. X.; Bai, Y.; Dang, D. B. *Cryst. Growth Des.* **2009**, *9*, 4362–4372. (b) Niu, J. Y.; Zhao, J. W.; Wang, J. P. *Inorg. Chem. Commun.* **2004**, *7*, 876–879.
(46) (a) Binnemans., K.; Görller-Walrand, C. *Chem. Phys. Lett.* **1995**, *235*, 163–174.(b) Carnall, W. T.; Goodman, G. L.; Rajnak, K.; Rana, R. S. *Argonne National Laboratory Report NL-88-8*; Argonne National Laboratory: Argonne, IL, 1988.
(47) (a) Yamase, T. *Chem. Rev.* **1998**, *98*, 307–325. (b) Papaconstantinou, E. *Chem. Soc. Rev.* **1989**, *18*, 1–31.
(48) (a) Xia, J.; Zhao, B.; Wang, H.-S.; Shi, W.; Ma, Y.; Song, H. B.; Cheng, P.; Liao, D. Z.; Yan, S. P. *Inorg. Chem.* **2007**, *46*, 3450–3458. (b) Lill, D. T.; Bettencourt-Dias, A.; Cahill, C. L. *Inorg. Chem.* **2007**, *46*, 3960–3965.
(49) (a) Xu, Q. H.; Li, L. S.; Liu, X. S.; Xu, R. R. *Chem. Mater.* **2002**, *14*, 549–555. (b) Yan, B.; Bai, Y. Y. *J. Fluoresc.* **2005**, *15*, 605–611.
(50) (a) Kuang, J. Y.; Liu, Y. L.; Zhang, J. X. *J. Solid State Chem.* **2006**, *179*, 266–269. (b) Meshova, S. B.; Kiriyaka, A. V.; Tsvirko, M. P.; Gorodnyuk, V. P. *J. Anal. Chem.* **2008**, *63*, 840–843.
(51) Sadakane, M.; Steckhan, E. *Chem. Rev.* **1998**, *98*, 219–237.
(52) (a) Xi, X. D.; Wang, G.; Liu, B. F.; Dong, S. J. *Electrochim. Acta* **1995**, *40*, 1025–1029. (b) Liu, L. Z.; Li, F. Y.; Xu, L.; Liu, X. Z; Gao, G. G. *J. Solid State Chem.* **2010**, *183*, 350–355.